Spin-Induced Forbidden Evanescent States in III-V Semiconductors

N. Rougemaille,[1] H.-J. Drouhin,[2] S. Richard,[3] G. Fishman,[3] and A. K. Schmid[1]
[1]*Lawrence Berkeley National Laboratory, Berkeley, California 94720, USA*
[2]*Laboratoire des Solides Irradiés, UMR 7642 CNRS & CEA/DSM/DRECAM, École Polytechnique, 91128 Palaiseau Cedex, France*
[3]*Institut d'Électronique Fondamentale, UMR 8622 CNRS, Université Paris Sud, 91405 Orsay Cedex, France*
(Received 26 November 2004; published 28 October 2005)

Within the band gap of a semiconductor no electronic propagating states are allowed, but there exist evanescent states which govern charge transport such as tunneling. In this Letter, we address the issue of their spin dependence in III-V semiconductors. Taking into account the spin-orbit interaction, we treat the problem using a $\boldsymbol{k} \cdot \boldsymbol{p}$ 14×14 Hamiltonian that we numerically compute for GaAs. Our results show that the removed spin degeneracy in the band gap can lead to giant energy splittings and induces forbidden zones in k space where evanescent states are suppressed.

DOI: 10.1103/PhysRevLett.95.186406 PACS numbers: 71.15.Ap, 73.20.At

According to Bloch theory, free electrons in a perfect periodic crystal behave like plane waves whose amplitude modulates with the period of the lattice. When a free electron reaches a surface or an interface, its wave function may be obtained by solving the Schrödinger equation at a given energy E, and by matching the allowed solutions on both sides of the boundary plane. As it was shown by Heine [1], the eigenvalues $E(\boldsymbol{k})$ of the crystal Hamiltonian can be expressed not only for real $\boldsymbol{k}$ wave vectors, but also for waves associated with complex $\boldsymbol{k}$. While real wave vectors describe propagating electron states, the imaginary part of $\boldsymbol{k}$ describes evanescent states, i.e., exponentially decaying wave functions. The dispersion relation $E(\boldsymbol{k})$ involving complex wave vectors is called complex band structure and describes how an electron will tunnel through a finite region of the crystal when its energy E lies in a band gap. The concept of complex band structure is particularly important when electronic properties of solid surfaces or interfaces are considered [2,3], and to determine tunneling states in semiconductor heterostructures and superlattices [4,5], magnetic tunnel junctions [6,7], or molecular electronic systems [8,9].

Contrary to diamond-type semiconductors like Si or Ge, zinc-blende-structure semiconductors lack a center of inversion. The spin-orbit interaction in these latter compounds removes the spin degeneracy of all energy bands (even in the absence of any external magnetic field) [10–13]. While the spin splitting of propagating electronic states is well established, the spin dependence of tunneling states is less well known. An interesting point was recently raised by Richard *et al.*, when they showed that no evanescent state associated with a purely imaginary wave vector can match the "real" conduction band of zinc-blende materials in the [110] direction [14]. In this Letter, we show that the removed spin degeneracy in this class of materials induces forbidden zones in the complex band structure in a wide range of crystallographic directions for both conduction and valence states, inside and outside the fundamental band gap. Moreover, from these forbidden zones result giant energy splittings, up to an order of magnitude larger than the splittings known in real band structure. These findings have deep consequences for tunneling transport and a careful mapping of the complex band structure in the band gap is a prerequisite to determine the evanescent states which can be sustained within a zinc-blende-type semiconducting barrier.

We compute complex band structure using a $\boldsymbol{k} \cdot \boldsymbol{p}$ technique through a 14×14 Hamiltonian (H_{14}) formalism. H_{14} can be computed for a large variety of structures; here we study GaAs as an example. We start from the $\boldsymbol{k} \cdot \boldsymbol{p}$ 14×14 Hamiltonian given in Ref. [15], which takes into account the valence bands (Γ_{7V}, Γ_{8V}), the first conduction band (Γ_{6C}) and the second conduction bands (Γ_{7C}, Γ_{8C}), schematically represented in Fig. 1 in the vicinity of the Γ point. H_{14} allows us to describe the first conduction band

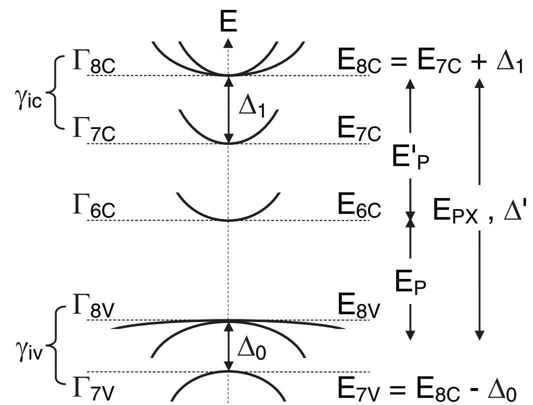

FIG. 1. Schematic band diagram of GaAs near the Γ point of the Brillouin zone. We use the notation of the T_d group to describe the valence bands (Γ_{7V}, Γ_{8V}), the first conduction band (Γ_{6C}) and the remote bands (Γ_{7C}, Γ_{8C}). The interband matrix elements of momentum (E_P, E_{PX}, E'_P) and of the spin-orbit interaction ($\Delta_0, \Delta_1, \Delta'$) are indicated. The Luttinger-like parameters γ_{iv} in the (Γ_{7V}, Γ_{8V}) levels and γ_{ic} in the (Γ_{7C}, Γ_{8C}) levels are also given.

 © 2005 The American Physical Society

and the valence bands with excellent accuracy over a wide part (about a fifth) of the first Brillouin zone. The crystal Hamiltonian H_{14} results from the substitution of a real wave vector with a complex wave vector. H_{14} is no longer Hermitian and $E(\boldsymbol{k})$ is only real along certain lines in the complex plane, the so-called "real lines" which join the real band structure at real $\boldsymbol{k}$ [1,16]. Because H_{14} takes into account both the lack of inversion symmetry and the spin-orbit interaction, it also removes the spin degeneracy of each band [15].

Before computing H_{14} numerically, it is instructive to consider the Γ_{6C} conduction band in the small-k approximation analytically. In that case, the spin splitting ΔE has k^3 dependence (Dresselhaus term) [10], and the Γ_{6C} energy levels can be written as $E_{\pm} = \gamma_C \bar{k}^2 \pm \Delta E$. In that expression, $\gamma_C = \hbar^2/2m^*$, $\bar{k}^2 = k_x^2 + k_y^2 + k_z^2$, and $\Delta E = \gamma\sqrt{k_x^2(k_y^2 - k_z^2)^2 + k_y^2(k_z^2 - k_x^2)^2 + k_z^2(k_x^2 - k_y^2)^2}$, where the constant γ describes the strength of the k-dependent internal magnetic field (D'yakonov-Perel' field), which removes the spin degeneracy [12]. Note that ΔE is maximum for $\boldsymbol{k}$ along the [110] direction and null for $\boldsymbol{k}$ along the [100] and [111] directions. For real wave vectors $\Delta E \geq 0$, but ΔE is not necessarily defined for complex $\boldsymbol{k}$, because the Dresselhaus term leads to an odd power of k in the initially spin degenerate, parabolic dispersion law. For example, for an imaginary wave vector k in the [110] direction $\Delta E = i\gamma\sqrt{2}k^3$ is an imaginary number. The imaginary value of ΔE implies that evanescent states are quenched in this direction. We emphasize that this "quenching" of the Γ_{6C} conduction states in the band gap originates in zinc-blende semiconductors from the combination of symmetry breaking and spin-orbit interaction, which leads to a nonzero value of γ. In contrast, for diamond-type semiconductors, $\gamma = \Delta E = 0$ in every crystallographic direction and complex wave vectors associated with the Γ_{6C} conduction states are always found in the band gap.

For the general case of larger k values and other bands (valence bands and upper conduction bands), no analytical expression of the energy levels can be written and one must compute the eigenvalues of H_{14}. To do that, we consider a surface (or interface) as a discontinuity where $\boldsymbol{k}_1$ and $\boldsymbol{k}_2$ are the components of the wave vector $\boldsymbol{k}_\parallel$ parallel to that discontinuity. Since the crystal Hamiltonian is invariant under translations parallel to the surface, only real values of these components are of interest. We can consider them as fixed parameters so that the energy is only a function of the complex vector $\boldsymbol{k}_\perp$ which describes the direction normal to the surface. To compute the eigenvalues of H_{14} numerically for GaAs and for $\boldsymbol{k}_\perp$, along the [100], [111], and [110] directions, the energy origin was taken at the top of the Γ_{8V} valence band. The parameters we use in the calculation, indicated in Fig. 1, are the following: the energy levels at the Γ point of the Γ_{8V}, Γ_{7V}, Γ_{6C}, Γ_{7C}, and Γ_{8C} bands are $E_{8V} = 0$ eV, $E_{7V} = -0.341$ eV, $E_{6C} = 1.519$ eV, $E_{7C} = 4.488$ eV, $E_{8C} = 4.659$ eV; the characteristic energies related to the interband matrix elements of momentum (spin-orbit interaction) between the $\{\Gamma_{8V}, \Gamma_{6C}\}$, $\{\Gamma_{8C}, \Gamma_{6C}\}$, and $\{\Gamma_{8V}, \Gamma_{8C}\}$ bands are $E_P = 22.5$ eV, $E'_P = 10.0$ eV, $E_{PX} = 15.0$ eV ($\Delta' = 0$ eV), respectively. The Luttinger-like parameters in the $(\Gamma_{7V}, \Gamma_{8V})$ levels are $\gamma_{1\nu} = 6.85$, $\gamma_{2\nu} = 2.10$, $\gamma_{3\nu} = 2.90$, and are set to 0 in the $(\Gamma_{7C}, \Gamma_{8C})$ levels (approximating remote bands as flat). This parameter set gives $\gamma = 24$ eV Å^3, which corresponds to the value used in Ref. [15].

First, we restrict the calculation to the case $\boldsymbol{k}_\parallel = 0$. The eigenvalues along the [100], [111], and [110] directions are presented in Figs. 2(a)–2(c), where $k_\perp$ is expressed in units of $2\pi/a$, a being the cubic lattice parameter ($a = 0.5653$ nm). Real and complex bands are plotted on the right and left sides of each panel. As expected [15], for real wave vectors the bands keep their twofold spin degeneracy in the [100] and [111] directions while the spin degeneracy is removed along the [110] direction. For imaginary wave

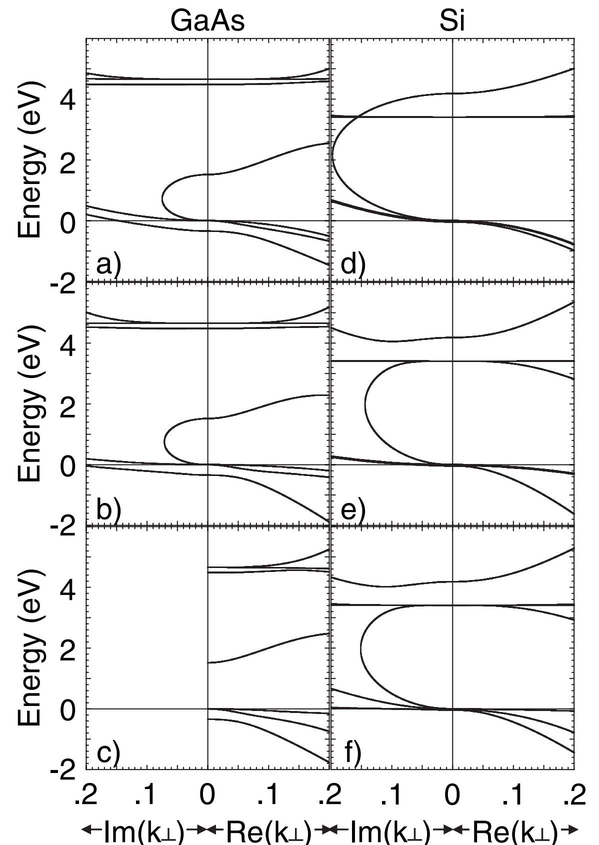

FIG. 2. Real and complex band structure of GaAs (left) and Si (right) along the (a),(d) [100], (b),(e) [111], and (c),(f) [110] directions. For the [100] and [111] directions, a loop-shaped complex band bridging the band gap connects the valence bands to the conduction bands. No such evanescent states are found in the [110] direction for GaAs (c), while they still exist in the case of Si (f).

vectors, the dispersion relations along the [100] and [111] directions are in agreement with those found in previous works [17–19], the main feature being a loop-shaped band that connects the first conduction band and the light-hole band. This band spans the entire band gap, which means that evanescent states can be found for all energies within the band gap. However, in the [110] direction where the spin degeneracy is removed, no evanescent states are obtained for any band. The numerical evaluation of H_{14} shows that the suppression of evanescent states is not limited to the energy region near the edge of Γ_{6C}, as we have shown analytically above. In fact, a free-electron wave propagating along the [110] direction cannot match any evanescent state in this direction, for all energies within the band gap.

This quenching of evanescent states originates from the combination of symmetry breaking in GaAs and spin-orbit interaction. The lack of a center of inversion in the crystal leads to a nonzero interaction between the Γ_{8C} and Γ_{6C} bands. This interaction, called E'_P in H_{14}, yields odd powers of k in the dispersion laws (Dresselhaus term for the Γ_{6C} band in the small-k approximation), independently of the strength of the spin-orbit coupling. E'_P then gives rise to possible imaginary contributions to the energy when complex wave vectors are considered. Because E'_P vanishes in crystals having a center of inversion, due to symmetry consideration, we do not expect any quenching of evanescent states in Si or Ge, for example. To ensure that this quenching is a direct consequence of the nonzero value of E'_P, we have computed H_{14} for Si. The parameters we used are the following: $E_{8V} = 0$ eV, $E_{7V} = -0.044$ eV, $E_{6C} = 4.185$ eV, $E_{7C} = E_{8C} = 3.410$ eV, $E_P = 25.0$ eV, $E'_P = 0$ eV, $E_{PX} = 15.0$ eV, $\Delta' = 0$ eV, $\gamma_{1\nu} = 4.285$, $\gamma_{2\nu} = 0.339$, $\gamma_{3\nu} = 1.446$, and $\gamma_{1c} = \gamma_{2c} = \gamma_{3c} = 0$. The results we find, plotted in Figs. 2(d)–2(f), permit direct comparison with the results reported in Ref. [18], where a tight-binding Hamiltonian had been used. The excellent quantitative agreement we find justifies our choice of the H_{14} Hamiltonian. Moreover, we note that for Si, complex bands are found in the all three low-index directions, including [110] [Figs. 2(d)–2(f)], contrary to GaAs. This fact points at the physical origin of evanescent state suppression in zinc-blende materials: within our formalism, the crucial difference between zinc-blende-semiconductors and diamondlike semiconductors is that in the former, the value of E'_P (which characterizes the momentum matrix element between the Γ_{8C} and Γ_{6C} bands) does not vanish. Supporting this picture we also checked that, if we artificially set $E'_P = 0$ for GaAs to simulate a center of inversion (while maintaining the other GaAs parameters unchanged), complex bands are again found in all directions.

For the general problem of tunneling transmission through a barrier, the components $(\boldsymbol{k}_1, \boldsymbol{k}_2)$ of the wave vector $\boldsymbol{k}_\parallel$ parallel to that barrier must be considered. For GaAs, we have determined the eigenstates of H_{14} for different $\boldsymbol{k}_\parallel$ values and $\boldsymbol{k}_\perp$ along the [100], [111], and [110] directions. For all $\boldsymbol{k}_\parallel \neq 0$ wave vectors we considered, $\Delta E \neq 0$ and the complex band structure exhibits astonishing properties. For example, to focus the discussion on a GaAs barrier grown along the [111] direction, no complex bands were found for $k_1 \neq 0$ ($k_1 \parallel [11-2]$) and evanescent states are suppressed for all values of k_2 ($k_2 \parallel [1-10]$) in the range studied here ($k_2 < 0.34$). The band structure in this range is similar to that shown in Fig. 2(c). In contrast, if $k_1 = 0$, complex bands always exist within the real band gap. It is instructive to visualize the complex band structure in 3D representations. The case $k_1 = 0$ is illustrated in Fig. 3 where the vertical axis represents energy (horizontal grid lines indicate $E = 0$), one horizontal axis represents the real and imaginary parts of $k_\perp$ to the right and to the left of vertical grid lines, respectively, and the second horizontal axis represents k_2 in the range of $0 < k_2 < 0.34$ ($2\pi/a$ units). The conduction band (Γ_{6C}) and the light-hole valence band (Γ_{8V}) are shown in purple while the heavy-hole valence band (Γ_{8V}) and the spin-orbit split valence band (Γ_{7V}) are in blue and green. To highlight the structure near the band gap, remote bands were omitted in this plot. For $k_2 = 0$ near the back of the 3D plot, the band gap between the real part of the conduction band and the real part of the light-hole valence band is bridged by a continuous, loop-shaped complex band. With $k_2 > 0$, the loop-shaped complex band develops a break near the top of

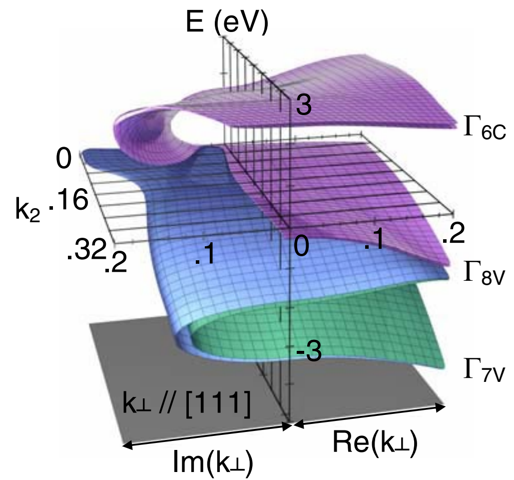

FIG. 3 (color online). 3D map of the GaAs complex band structure in the [111] direction. The vertical axis represents energy and one horizontal axis represents the real (right side) and imaginary (left side) parts of $k_\perp$. $k_1 = 0$ ($k_1 \parallel [11-2]$) and k_2 ($k_2 \parallel [1-10]$) is varied from 0 to 0.34 along the second horizontal axis. The conduction band (Γ_{6C}) and the light-hole valence band (Γ_{8V}) are shown in purple while the heavy-hole valence band (Γ_{8V}) and the spin-orbit split valence band (Γ_{7V}) are in blue and green. To emphasize the extension of forbidden zones for evanescent states, the 3D map is oriented so that the origin is near the back of the plot.

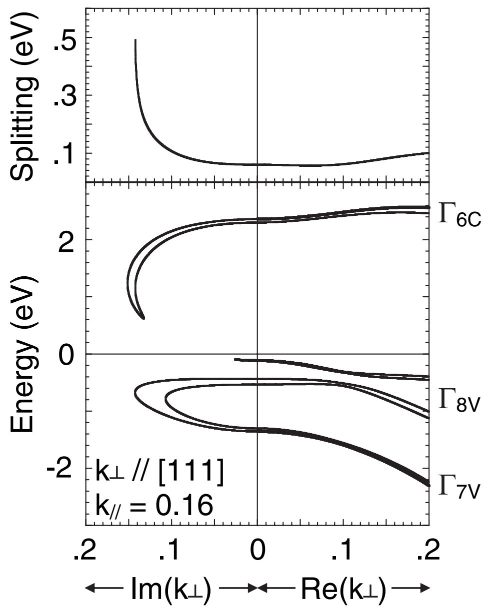

FIG. 4. Top: values of the spin splitting of the Γ_{6C} conduction band in the [111] direction as a function of $k_\perp$ for $k_1 = 0$ and $k_2 = 0.16$. Bottom: real (right panel) and complex (left panel) band structure, plotted for the same range of $k_\perp$ values.

the light-hole valence band and a zone appears where both the real and the complex part of the band structure exhibit a gap in the same energy range. This means that the real band gap is also free of complex bands in this region, i.e., this is a forbidden zone where neither propagating electronic states nor evanescent states can exist in this crystal direction. Similar results are obtained in the [110] and [100] directions when $k_\parallel \neq 0$. These results show that the spin-orbit interaction in zinc-blende-type semiconductors has dramatic consequences on the complex band structure in all crystallographic directions. This is crucially important to describe tunneling phenomena: depending on the surface orientation and the wave vector involved, the tunneling transmission through a III-V semiconductor barrier may be essentially suppressed.

The loop-shaped complex bands have additional astonishing properties. The loops contain regions of diverging dispersion $\partial E/\partial k$ which, in combination with removed spin degeneracy, lead to a region in k space where the energy splitting can reach extremely high values. For example, the 2D complex band structure corresponding to the case $k_2 = 0.16$ in Fig. 3 and the associated energy splitting of the Γ_{6C} conduction band are shown in Fig. 4. For $\mathrm{Im}(k_\perp) = 0.15$, near the middle of the band gap, the energy splitting reaches 0.5 eV: this value is almost 1 order of magnitude higher than the energy splitting observed for $k_\perp$ with real values of similar magnitude. As far as we know, such giant splittings have not been reported so far. Moreover, the nonzero value of the energy splitting in the band gap for very small $k_\perp$ is a pure spin splitting, and may be used to inject 100% spin-polarized carriers through a [111]-orientated GaAs barrier with a transmission close to unity. Combining the possibility of quenching tunneling electron transport in III-V semiconductor barriers and the possibility of taking advantage of giant spin splittings can serve as a basis for future spin-injection, spin-filtering, or other spin-dependent tunneling devices.

We thank A. Bournel, C. Bouton-Drouhin, J.-N. Chazalviel, M. Lombardi, and R. M. Couto for useful discussions. H.-J. D. acknowledges the Délégation Générale pour l'Armement for support.

[1] V. Heine, Proc. Phys. Soc. London **81**, 300 (1963).
[2] R. O. Jones, Proc. Phys. Soc. London **89**, 443 (1966).
[3] F. Forstmann and V. Heine, Phys. Rev. Lett. **24**, 1419 (1970).
[4] G. Bastard, *Wave Mechanics Applied to Semiconductor Heterostructures*, Les Éditions de Physique (Les Ulis, France, 1996).
[5] M. F. Schuurmans and G. W. 't Hooft, Phys. Rev. B **31**, 8041 (1985).
[6] Ph. Mavropoulos, N. Papanikolaou, and P. H. Dederichs, Phys. Rev. Lett. **85**, 1088 (2000).
[7] X.-G. Zhang and W. H. Butler, J. Phys. Condens. Matter **15**, R1603 (2003).
[8] J. K. Tomfohr and O. F. Sankey, Phys. Rev. B **65**, 245105 (2002).
[9] H. Wang, J. P. Lewis, and O. F. Sankey, Phys. Rev. Lett. **93**, 016401 (2004).
[10] G. Dresselhaus, Phys. Rev. **100**, 580 (1955).
[11] E. O. Kane, J. Phys. Chem. Solids **1**, 249 (1957).
[12] M. I. D'yakonov and V. I. Perel', Zh. Eksp. Teor. Fiz. **60**, 1954 (1971) [Sov. Phys. JETP **33**, 1053 (1971)].
[13] M. Cardona, N. E. Christensen, and G. Fasol, Phys. Rev. B **38**, 1806 (1988).
[14] S. Richard *et al.*, J. Appl. Phys. **97**, 083706 (2005).
[15] P. Pfeffer and W. Zawadzki, Phys. Rev. B **53**, 12 813 (1996).
[16] E. I. Blount, *Solid State Physics*, Appendix C, edited by F. Seitz and D. Turnbull (Academic, New York, 1962), Vol. 13.
[17] J. N. Schulman and T. C. Mc Gill, in *Synthetic Modulated Structure Materials*, edited by L. L. Chang and B. C. Giessen (Academic, New York, 1984).
[18] Y.-C. Chang, Phys. Rev. B **25**, 605 (1982).
[19] T. B. Boykin, Phys. Rev. B **54**, 8107 (1996).